Solvent mediated interactions close to fluid-fluid phase separation: microscopic treatment of bridging in a soft core fluid

A.J. Archer* and R. Evans

H. H. Wills Physics Laboratory, University of Bristol, Bristol BS8 1TL, UK

R. Roth and M. Oettel

Max-Planck-Institut für Metallforschung,

Heisenbergstr. 3, 70569 Stuttgart, Germany and

ITAP, Universität Stuttgart, Pfaffenwaldring 57, 70569 Stuttgart, Germany

(Dated: February 2, 2008)

Abstract

Using density functional theory we calculate the density profiles of a binary solvent adsorbed around a pair of big solute particles. All species interact via repulsive Gaussian potentials. The solvent exhibits fluid-fluid phase separation and for thermodynamic states near to coexistence the big particles can be surrounded by a thick adsorbed 'wetting' film of the coexisting solvent phase. On reducing the separation between the two big particles we find there can be a 'bridging' transition as the wetting films join to form a fluid bridge. The potential between the two big particles becomes long ranged and strongly attractive in the bridged configuration. Within our mean-field treatment the bridging transition results in a discontinuity in the solvent mediated force. We demonstrate that accounting for the phenomenon of bridging requires the presence of a non-zero bridge function in the correlations between the solute particles when our model fluid is described within a full mixture theory based upon the Ornstein-Zernike equations.

PACS numbers:

I. INTRODUCTION

Big solute particles (e.g. colloids) immersed in a solvent of smaller particles interact with each other by an effective potential which is the sum of their direct interaction and a solvent mediated (SM) potential. Even when the direct interaction consists solely of two–body terms, the SM potential contains higher body contributions, of all orders which are determined formally by integrating out the solvent degrees of freedom. This conceptual framework yields, in principle, a much simpler effective Hamiltonian which involves only the coordinates of the big particles.[1] In certain systems the two–body term in the SM potential may dominate completely the corresponding direct interaction. A well–known example is a suspension of big hard–sphere colloids in a solvent of small hard–spheres. There the SM potential between the colloids is termed the depletion interaction and this is the only contribution to the effective potential for separations greater than the big hard–sphere diameter.[2] In the case of a (non–hard) solvent which is at a state point near to fluid-fluid phase separation, big solute particles can be surrounded by a thick adsorbed 'wetting' film of the coexisting solvent phase.[3] If two such big particles become sufficiently close, there can be a 'bridging transition' as the wetting films surrounding the two big particles join to form a fluid bridge of the wetting phase – see for example Ref. 4 and references therein. In wet granular media these bridging (or capillary) forces lead to strong and very short–ranged interactions. For small solutes these effective attractions become rather long–ranged with respect to the dimension of the solute as is known from tip–substrate interactions in atomic force microscopy.[5] Long–ranged attractive interactions are also surmised for hydrophobic molecules in water at ambient conditions.[6] Bridging is also a possible mechanism for driving colloidal flocculation.[7]

In previous work,[8,9] the wetting of a binary solvent around a single big particle and the influence of these thick adsorbed films on the effective SM potential between two big particles, was investigated for a particular model fluid, namely the generalisation to mixtures of the Gaussian core model (GCM).[1,8,9,10,11,12,13,14,15,16,17,18] A Gaussian potential provides a good approximation for the effective potential between the centres of mass of polymers in solution.[1,19,20] The approach to calculating the SM potentials was based upon the theory developed by Roth *et al.*[2] – henceforth referred to as the 'insertion method'. The insertion method works within the framework of density functional theory (DFT)[21] and uses as input

the density profiles calculated around a *single* big particle in order to calculate the SM potential between a *pair* of big particles.[2,8,9] Although the insertion method is formally exact, in practice one must employ an approximation for the free energy functional of the mixture of big and small particles.[2] For state points near to coexistence we found thick adsorbed films around the big particles resulting in long ranged, strongly attractive SM potentials whose range was determined by the thickness of the wetting film. However, using the insertion method, we were unable to detect any direct sign of bridging in the SM potential.[8,9]

The present work can be viewed as going a significant step further than Refs. 8,9. Here we investigate the same system: two large solute Gaussian particles, immersed in a binary GCM solvent near to phase separation. However, whereas the previous work used the elegant insertion method, the present work can be viewed as the 'brute-force' approach to the problem. Using an accurate DFT for the binary GCM solvent of small particles[1,8,9,16,17] we calculate explicitly the solvent density profiles around a fixed *pair* of the big GCM particles, treating the latter as external potentials, and determine the resulting grand potential. By repeating this calculation for a range of values of the separation between the centres of the two big particles we obtain the SM potential. We find, within the present (mean-field) DFT approach, that when thick adsorbed films are present there can be a bridging transition as the separation between the two big particles is decreased, i.e. the formation of a bridging configuration gives rise to a discontinuity in the derivative of the SM potential. We believe that this is the first time a non-local DFT has been used to calculate bridging density profiles and the resulting effective potential between two particles. Bridging has been investigated previously within coarse-grained, local DFT in the recent study of Stark *et al.*[22] for big hard spherical colloids immersed in an isotropic liquid crystal host close to the isotropic-nematic phase boundary. Similarly, Andrienko *et al.*[23] calculated bridging density profiles of a solvent adsorbed between a big colloid and a planar wall using a local DFT.

We also investigate the SM potential between two big GCM particles in a region of the solvent phase diagram near the binodal but lying outside the single particle thin-thick adsorbed film transition line,[9] where a single big particle does not have a thick adsorbed 'wetting' film of the coexisting solvent phase around it. Adsorption still influences strongly the SM potential. We find an analogue of capillary condensation; as the two big particles become sufficiently close, the composite object is large enough to induce condensation of the coexisting solvent phase around the *pair* of big particles. This effect is somewhat different

from that which can occur between two big hard-core particles in a solvent near to coexistence. When a pair of such particles are sufficiently close, a bridge of the coexisting phase can condense in the gap between the two big particles, without there being thick 'wetting' films adsorbed on each of the big particles.[4] In the present soft core system the strong adsorption is not confined to the space between the big particles, rather it extends through the whole region in which the two big particles are situated. This local condensation also results in a jump in the SM force between the two big particles with the SM potential becoming strongly attractive for small separations.

In the final part of the present work we relate our results for the SM potential to an approach for calculating the SM potential based upon the mixture Ornstein-Zernike (OZ) equations.[26,27,28] By solving the OZ equations together with a closure relation one can calculate the various fluid correlation functions. It is well known that if one makes a diagrammatic expansion for the fluid correlation functions the hyper-netted chain (HNC) closure approximation neglects a certain class of (bridge) diagrams which, taken together, is termed the bridge function.[26] We show that in order to account for the phenomenon of bridging of solvent between big particles within an OZ approach to the fluid structure, one must incorporate an accurate theory for the bridge-diagrams.

The paper is laid out as follows: In Sec. II we describe briefly our model fluid, the GCM, and the DFT used to calculate the solvent density profiles and the SM potential between two big solute GCM particles. Section III presents results for the density profiles and SM potentials in the regime where there are thick adsorbed films around a single big particle resulting in a bridging transition when two big particles are sufficiently close together. In Sec. IV we present a simple analytic 'capillarity' approximation which describes qualitatively the onset of the bridging transitions that we find. Section V describes the effect of the formation of a thick adsorbed film around a *pair* of big particles, in the portion of the phase diagram where there is no thick film around a single big particle and Sec. VI describes our demonstration that bridging between big particles is related to the bridge-function. Finally, in Sec. VII, we discuss our results and draw some conclusions.

II.   MODEL FLUID AND SM POTENTIALS

We determine the SM potential between two big (B) Gaussian particles immersed in a binary solvent of smaller Gaussian particles. The GCM, in which the particles of species i and j interact via purely repulsive Gaussian potentials

$$v_{ij}(r) = \epsilon_{ij} \exp(-r^2/R_{ij}^2), \tag{1}$$

is a simple model for polymers in solution[1,12,13,16,17,20] (in particular, Ref. 1 provides a good general introduction to the GCM). For the binary GCM solvent we choose pair potential parameters corresponding to a binary mixture of polymers of length ratio 2:1, as were used in previous work on this model fluid.[8,9,16,17] The values are $R_{22}/R_{11} = 0.665$, $R_{12}/R_{11} = 0.849$, $\beta\epsilon_{11} = \beta\epsilon_{22} = 2.0$ ($\beta = 1/k_BT$) and $\epsilon_{12}/\epsilon_{11} = 0.944$. R_{11} is the basic length scale in the system. For this choice of parameters the binary mixture exhibits fluid-fluid phase separation. The phase diagram of this binary solvent is plotted in the total density, $\rho^0 = \rho_1^0 + \rho_2^0$, versus concentration, $x = \rho_2^0/\rho^0$, plane in Fig. 1 (ρ_ν^0 are the bulk densities of the small particles of species $\nu = 1, 2$) – see also Ref. 16.

The SM potential between two big particles, labelled A and B, with centres at $\mathbf{r}_A$ and $\mathbf{r}_B$, separated by a distance h, is given by the difference in the grand potential:

$$W_{AB}(h) = \Omega(|\mathbf{r}_A - \mathbf{r}_B| = h) - \Omega(|\mathbf{r}_A - \mathbf{r}_B| = \infty). \tag{2}$$

This result can be re-expressed (trivially) in terms of excess grand potentials, $\omega_{ex}^i \equiv \Omega - \Omega_b$, where $i = A, B$ and Ω_b is the grand potential of the bulk solvent in the situation where there are no big particles present. Then,

$$W_{AB}(h) = \omega_{ex}^{AB}(|\mathbf{r}_A - \mathbf{r}_B| = h) - \omega_{ex}^A - \omega_{ex}^B. \tag{3}$$

Note that ω_{ex}^i, the excess grand potential for inserting a single big particle of species i, is equal to μ_{ex}^i, the excess chemical potential of big species i in the limit of the bulk density of this species $\rho_i^0 \to 0$.[2,8,9] The effective pair potential between two identical big particles is then the sum of the bare interaction $v_{BB}(r)$ and the SM potential:

$$v_{BB}^{eff}(h) = v_{BB}(h) + W_{BB}(h). \tag{4}$$

Recall also, that

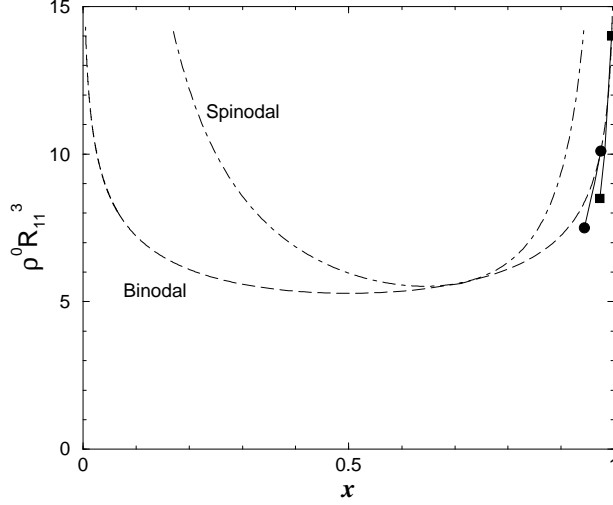$$v_{BB}^{eff}(h) = -k_BT \ln g_{BB}(h), \tag{5}$$

FIG. 1: The bulk phase diagram for a binary mixture of GCM particles with $\epsilon_{12}/\epsilon_{11} = 0.944$ and $R_{22}/R_{11} = 0.665$, equivalent to a mixture of two polymers with length ratio 2:1 (see also Ref. 16). ρ^0 is the total density and x is the concentration of the smaller species 2. The solid line whose ends are denoted by filled circles is the thin-thick adsorbed film transition of the binary fluid adsorbed around a *single* big GCM particle with pair potential parameters $\beta\epsilon_{B1} = 1.0$, $\beta\epsilon_{B2} = 0.8$, $R_{B1}/R_{11} = 5.0$ and $R_{B2}/R_{11} = 4.972$ – see Ref. 9. It meets the binodal at the 'wetting point' (upper circle) with $x = 0.975$ and $\rho^0 R_{11}^3 = 10.1$ (note these values differ slightly from the result quoted in Ref. 9 – see footnote[30]) and terminates at a critical point (lower circle) with $x = 0.94$ and $\rho^0 R_{11}^3 = 7.5$. The solid line whose ends are denoted by filled squares is the thin-thick adsorbed film transition of the binary fluid adsorbed around a composite *pair* of the same big GCM particles at zero separation $h = 0$. This transition line meets the binodal (upper square) at $x = 0.995$ and $\rho^0 R_{11}^3 = 14$ and terminates at a critical point (lower square) with $x = 0.973$ and $\rho^0 R_{11}^3 = 8.5$.

where g_{BB} is the big-big radial distribution function in the limit of the big particle bulk density $\rho_B^0 \to 0$. In the present work we use DFT to obtain the quantities $\omega_{ex}^{AB}(|\mathbf{r}_A - \mathbf{r}_B| = h)$ and ω_{ex}^i.

In DFT one calculates the solvent one body density profiles, $\{\rho_\nu(\mathbf{r})\}$, for a given set of external potentials, $\{V_\nu(\mathbf{r})\}$, by minimising the grand potential functional:[21]

$$\Omega_V[\{\rho_\nu\}] = \mathcal{F}_{id}[\{\rho_\nu\}] + \mathcal{F}_{ex}[\{\rho_\nu\}] - \sum_\nu \int d\mathbf{r}\, \rho_\nu(\mathbf{r})\, [\mu_\nu - V_\nu(\mathbf{r})], \qquad (6)$$

where μ_ν are the chemical potentials for the two species, $\nu = 1, 2$, of solvent particles. The

ideal gas part of the intrinsic Helmholtz free energy functional is

$$\mathcal{F}_{id}[\{\rho_\nu\}] = k_B T \sum_\nu \int d\mathbf{r} \; \rho_\nu(\mathbf{r}) \, [\ln(\Lambda_\nu^3 \rho_\nu(\mathbf{r})) - 1], \tag{7}$$

where Λ_ν is the thermal de Broglie wavelength of species ν, and $\mathcal{F}_{ex}[\{\rho_\nu\}]$ is the excess part of the intrinsic Helmholtz free energy functional. Minimising (6) together with (7) one obtains the Euler-Lagrange equation

$$0 = k_B T \ln \Lambda_\nu^3 \rho_\nu(\mathbf{r}) - k_B T c_\nu^{(1)}(\mathbf{r}) - \mu_\nu + V_\nu(\mathbf{r}), \tag{8}$$

where

$$c_\nu^{(1)}(\mathbf{r}) = -\beta \frac{\delta \mathcal{F}_{ex}[\{\rho_\nu\}]}{\delta \rho_\nu(\mathbf{r})}, \tag{9}$$

is the one body direct correlation function, which is a functional of $\{\rho_\nu\}$. In an exact treatment the density profiles $\{\rho_\nu\}$ satisfying (8) would yield the exact grand potential Ω as the minimum of Ω_V.[21] At this point we also recall that the two-body direct correlation functions are given by the second functional derivative[21]

$$c_{\nu,\xi}^{(2)}(\mathbf{r}, \mathbf{r}') = -\beta \frac{\delta^2 \mathcal{F}_{ex}[\{\rho_\nu\}]}{\delta \rho_\nu(\mathbf{r})\delta \rho_\xi(\mathbf{r}')}. \tag{10}$$

For the GCM the following approximate excess Helmholtz free energy functional turns out, despite its simplicity, to be remarkably accurate at high densities $\rho^0 R_{11}^3 \gtrsim 5$:[1,9,12,13,16,29]

$$\mathcal{F}_{ex}^{RPA}[\{\rho_i\}] = \frac{1}{2} \sum_{\nu,\xi} \int d\mathbf{r} \int d\mathbf{r}' \; \rho_\nu(\mathbf{r}) \, \rho_\xi(\mathbf{r}') v_{\nu,\xi}(|\mathbf{r} - \mathbf{r}'|), \tag{11}$$

where $v_{\nu,\xi}(r)$ is the pair potential between the small solvent particles of species ν and ξ, given by Eq. (1). The functional, Eq. (11), is that which generates the RPA closure: $c_{\nu,\xi}^{(2),RPA}(\mathbf{r}, \mathbf{r}') = -\beta v_{\nu,\xi}(|\mathbf{r} - \mathbf{r}'|)$, for the pair direct correlation functions.[1,12,13,16] The higher the density, the more accurate is the RPA for this soft core model.[1]

In the present work we choose the external potential to correspond to two fixed big Gaussian particles of the same size, separated by a distance h:

$$V_\nu(\mathbf{r}) = \epsilon_{B\nu} \exp(-(\mathbf{r} + \mathbf{h}/2)^2/R_{B\nu}^2) + \epsilon_{B\nu} \exp(-(\mathbf{r} - \mathbf{h}/2)^2/R_{B\nu}^2), \tag{12}$$

with $\nu = 1, 2$ and where $\mathbf{h}$ is a vector along the z-axis, with $|\mathbf{h}| = h$, i.e. the centres of the big particles are at $z = \pm h/2$. Throughout the present study we choose the external potential parameters to be $\beta \epsilon_{B1} = 1.0$, $\beta \epsilon_{B2} = 0.8$, $R_{B1}/R_{11} = 5.0$ and $R_{B2}/R_{11} = 4.972$,
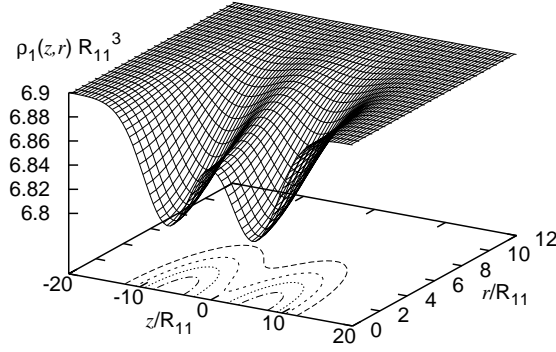
FIG. 2: The density profile of a one component fluid of Gaussian particles, with bulk density $\rho_1^0 R_{11}^3 = 6.9$, around a pair of big Gaussian particles, whose centres are located on the z-axis a distance $h/R_{11} = 12$ apart. The contours in the $z - r$ plane correspond to $\rho_1(z, r) = 6.82, 6.84, 6.86$ and 6.88.

the same values as those used for the big-small particle pair potentials in much of the work in Refs. 8,9. With this external potential the solvent density profiles have cylindrical symmetry – i.e. the density profiles are functions $\rho_\nu(z, r)$, where the z-axis runs through the centres of the two big particles, and r is the radial distance from the z-axis. If the external potential on the solvent were exerted by hard particles, special care would be required to ensure that the hard boundary is compatible with the grid of the numerical calculations in order to avoid numerical artefacts in the contact density.[25] One would have to employ either matching coordinate systems, such as the bispherical one used, e.g., in Refs. 22 and 24, or even more sophisticated finite-element methods with adaptive mesh-size.[23] One of the appealing features of the *soft core* GCM used in the present investigation is that we can avoid this problem and perform our calculations on a cartesian grid in cylindrical coordinates.

In Fig. 2 we display a typical density profile for a one component solvent of particles of species 1, with the external potential given by Eq. (12) with $h/R_{11} = 12$. Having calculated the solvent density profiles for a given separation h of big particles, we can insert these into Eq. (6) to calculate the (excess) grand potential and the SM potential $W_{BB}(h)$ from Eq. (3). In Fig. 3 we display the SM potential between two big GCM particles, calculated for a one component solvent with bulk density $\rho_1^0 R_{11}^3 = 6.9$, i.e. the state point corresponding to the profiles in Fig. 2. Figure 3 should be compared with Fig. 2 of Ref. 9. The open circles are

8

the results from the present 'brute-force' calculation. The solid line is the result obtained using the insertion method, where one calculates only the solvent density profiles around an islolated, single big particle and then uses the general result[2]

$$\beta W_{BB}(h) \; = \; c_B^{(1)}(h \to \infty; \rho_B^0 \to 0) \; - \; c_B^{(1)}(h; \rho_B^0 \to 0), \tag{13}$$

i.e. one calculates the difference in the excess chemical potential between inserting the second big particle a distance h from the first and inserting it at $h = \infty$. As emphasised in the Introduction, Eq. (13) is formally exact when we know the exact free energy functional for a mixture of big and small particles. Here we use the same RPA functional (11) extended to include a third species B, in order to find an approximate $c_B^{(1)}$ in Eq. (13) – see Ref. 9 for more details. The results from the two different routes are almost indistinguishable for this point in the phase diagram, and generally for other state points where no thick adsorbed (wetting) films are present around the big particles. The dashed line in Fig. 3 corresponds to the analytic approximation for $W_{BB}(h)$ presented in Ref. 9:

$$\beta W_{BB}^{pure}(h) \; = \; -(\pi/2)^{3/2} \beta \epsilon_{B1} \rho^* R_{B1}^3 \exp(-h^2/2R_{B1}^2), \tag{14}$$

where $\rho^* \; = \; \rho_1^0 \beta \epsilon_{B1}/(1 + \pi^{3/2} \beta \epsilon_{11} R_{11}^3 \rho_1^0)$. The agreement between this approximation and the result of the full numerical DFT calculations is remarkably good.

III. THE SM POTENTIAL WHEN THERE ARE THICK ADSORBED FILMS: BRIDGING

We now consider the case when thick adsorbed films develop around the big GCM particles. The circumstances in which this can occur are discussed in Refs. 8,9. In general there can be thick adsorbed films when the small solvent particles are in a state near to phase separation. For the present mixture, the big GCM particles favour species 1 of the small solvent particles, and so thick adsorbed films of the coexisting phase rich in species 1 can develop when the big particles are immersed in the solvent at a state point lying on the right hand side of the binodal, which is poor in species 1. In Refs. 8,9 it was found that thick films develop via a thin-thick transition out of bulk coexistence. The locus of these transitions is shown as the solid line joining filled circles in Fig. 1. Note that this transition line meets the binodal at a 'wetting point' whose density is somewhat higher than that quoted
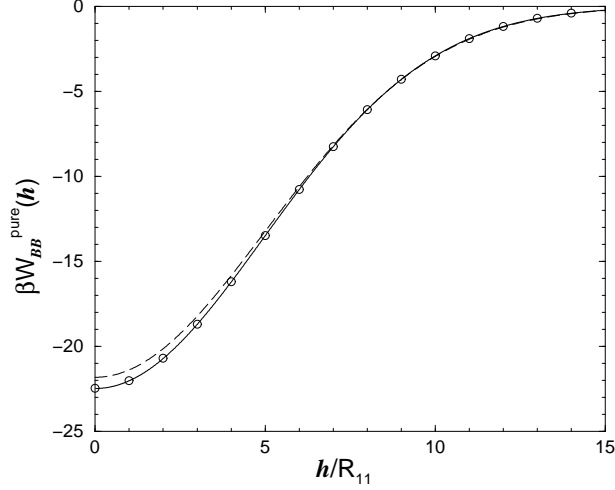
FIG. 3: The SM potential between two big GCM particles in a one component solvent of small GCM particles, with bulk density $\rho_1^0 R_{11}^3 = 6.9$. h is the separation between the two big particles. The solid line is the DFT insertion method results, the open circles are the results from the present 'brute-force' calculation (the two are almost indistinguishable) and the dashed line is the analytic result, Eq. (14), obtained in Ref. 9.

in Ref. 9. This discrepancy is associated with the existence of metastable minima in the free energy.[30] In Figs. 4 and 5 we display density profiles calculated for a pair of big particles immersed in a binary solvent of small GCM particles with bulk density $\rho^0 R_{11}^3 = 8.5$ and concentration $x = 0.948$, a state point near to coexistence, located inside the single particle thin-thick adsorbed film transition line (see Fig. 1). (Fig. 6 of Ref. 9 displays the solvent density profiles around a *single* big particle for this state point.) In Figs. 4 and 5 the centres of the big particles are a distance $h/R_{11} = 17$ apart and there are thick adsorbed wetting films around the big particles. However, in Fig. 4 there is a fluid bridge between the two particles whereas in Fig. 5, there is no fluid bridge. This second set of profiles corresponds to a metastable situation. For this state point the bridging transition occurs at a slightly larger separation $h_t/R_{11} = 17.4$; this is where the bridged and unbridged configurations have equal grand potential. In Fig. 6 we display the SM potential $W_{BB}(h)$ for this state point. There are two distinct branches, corresponding to bridged and non-bridged configurations. For $h > h_t$ the unbridged configuration is the stable one, whereas for $h < h_t$ the bridged configuration becomes stable. Since the two branches of $W_{BB}(h)$ have different slopes there is a discontinuity in the SM force, $-\mathrm{d}W_{BB}(h)/\mathrm{d}h$, at h_t, the separation where the transition

occurs. The extent of the metastable portions is substantial; these extend well beyond the equilibrium transition. This type of metastability, with accompanying hysteresis, was also found by Stark *et al.*[22] in their recent study of the bridging of the nematic wetting film between two colloids immersed in the isotropic phase of a liquid crystal. We display in Fig. 7 the SM potential calculated in the same way for a different point in the phase diagram, closer to the solvent bulk critical point, at a total density $\rho^0 R_{11}^3 = 6.9$ and concentration $x = 0.88$. This state point is also near to bulk coexistence (see Fig. 1). In both figures 6 and 7 we compare the SM potential calculated using the present 'brute-force' approach (solid lines) with the results obtained using the insertion method (dashed line) as described in Ref. 9. There is a significant difference between the results from the two methods; the insertion method does not capture the existence of two distinct branches of the grand potential. Thus it does not appear to include explicitly the effects of a bridging transition. The insertion method does predict very strongly attractive SM potentials, of a similar magnitude to those from full DFT, but does not yield the correct shape or range for $W_{BB}(h)$. In contrast we recall from Sec. II that in the regime where there are no thick adsorbed films, the results from the insertion method and the 'brute-force' method are in good agreement.

IV. APPROXIMATE MODEL FOR THE SM POTENTIAL WHEN BRIDGING OCCURS

In Ref. 9 we found that when there was a thick adsorbed film around a single big particle, a good approximation for the excess grand potential of a *single* big GCM particle immersed in a binary GCM solvent of small particles is:

$$\omega_{ex}^B \simeq \sum_{\nu=1}^{2} \pi^{3/2} \epsilon_{B\nu} R_{B\nu}^3 \rho_\nu^{coex} + 4\pi l^2 \gamma(l), \tag{15}$$

where ρ_ν^{coex} are the solvent bulk densities in the coexisting phase, i.e. the phase that forms the adsorbed film. l is the thickness of the adsorbed film ($l \sim R_{B\nu}$, but we determine its value by calculating explicitly via DFT, the density profiles around a single big particle) and $\gamma(l)$ is the fluid-fluid surface tension, which we approximate by $\gamma(\infty)$, the surface tension of the planar free interface (this is calculated using the approach presented in Ref. 16). The first term in Eq. (15) is the excess grand potential for inserting a single big particle into the coexisting phase, obtained from the RPA bulk equation of state,[9] and the second term is the
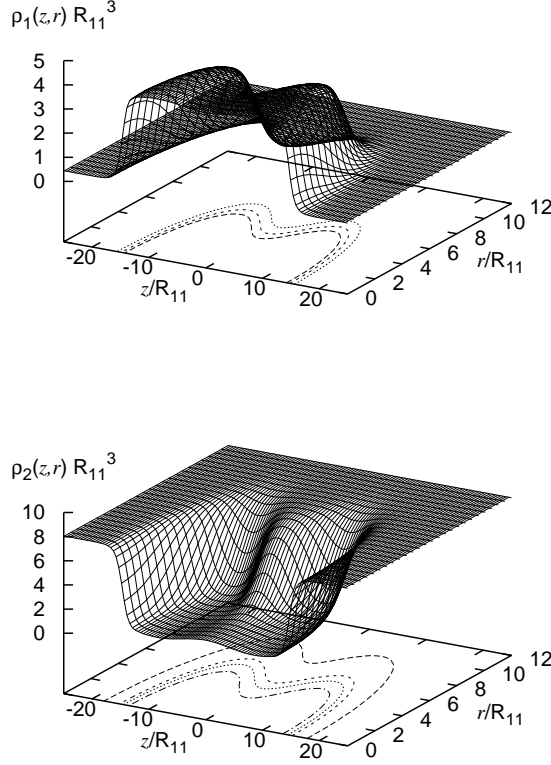
FIG. 4: Density profiles $\rho_\nu(z,r)$, $\nu = 1,2$, for a solvent with total density $\rho^0 R_{11}^3 = 8.5$ and concentration $x = 0.948$, a state near to phase separation located inside the single particle thin-thick adsorbed film transition line (see Fig. 1). The centres of the big particles are a distance $h/R_{11} = 17$ apart. Note the presence of thick adsorbed (wetting) films and the fluid bridge between the particles. The contours, plotted in the $z - r$ plane, correspond to $\rho_1(z,r)R_{11}^3 = 1$, 2 and 3 and $\rho_2(z,r)R_{11}^3 = 2$ to 8 in increments of 2. The bridged configuration is the stable one for this value of h/R_{11}.

contribution from forming a spherical fluid-fluid interface. Generalising to two big particles we might therefore expect the following approximation to be reliable:

$$\omega_{ex}^{BB}(h) \simeq 2\sum_{\nu=1}^{2} \pi^{3/2}\epsilon_{B\nu}R_{B\nu}^3\rho_\nu^{coex} \; + \; A(l,h)\gamma'(l,h), \tag{16}$$

where $A(l,h)$ is the surface area of the fluid-fluid interface between the adsorbed film of the phase rich in species 1 which develops around the two big particles and the bulk fluid rich in species 2. $\gamma'(l,h)$ is the surface tension, which we again approximate by $\gamma(\infty)$, the
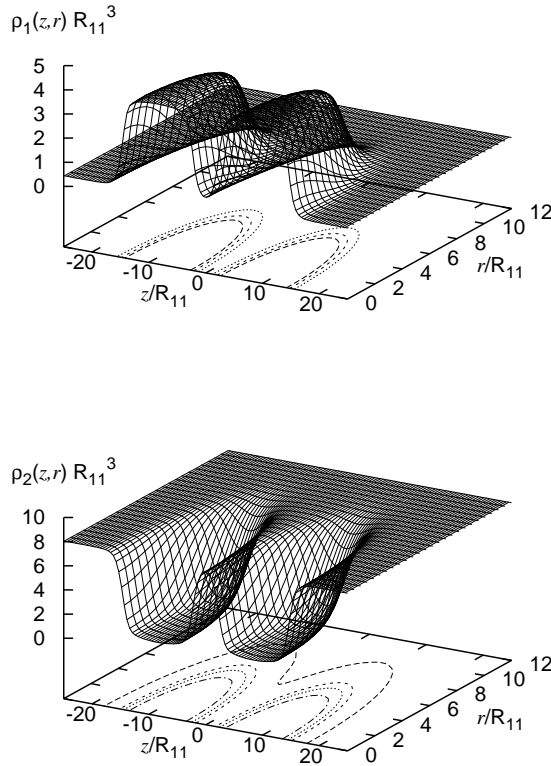
12

FIG. 5: Density profiles for the same state point and separation, $h/R_{11} = 17$, as Fig. 4, but now there is no fluid bridge between the big particles. This configuration is metastable.

planar fluid-fluid interfacial tension. A similar sharp-kink or capillarity approach was used in Ref. 4 to investigate bridging for very big hard-core solute particles that induce thick adsorbed (wetting) films but some new features arise for soft core systems. At first sight we might expect the first (single particle insertion) term in Eq. (16) to be inaccurate as $h \to 0$, when the big particles are strongly overlapping. However, this is not the case. When $h = 0$ the first term in Eq. (16) is accurate, since two big particles lying on top of each other result in an external potential that has the same form as that due to a single big particle with $\epsilon_{B\nu}$ twice the value for one of the big particles taken alone. In other words, if we take the first term in Eq. (15) and make the substitution $\epsilon_{B\nu} \to 2\epsilon_{B\nu}$, then we obtain the the same first term as in Eq. (16). Given this observation the first term in (16) should be accurate for both large h and for $h = 0$. Thus, by 'continuity' we expect it to be accurate for all values of h. The overall accuracy of Eq. (16) should depend upon how accurately we determine
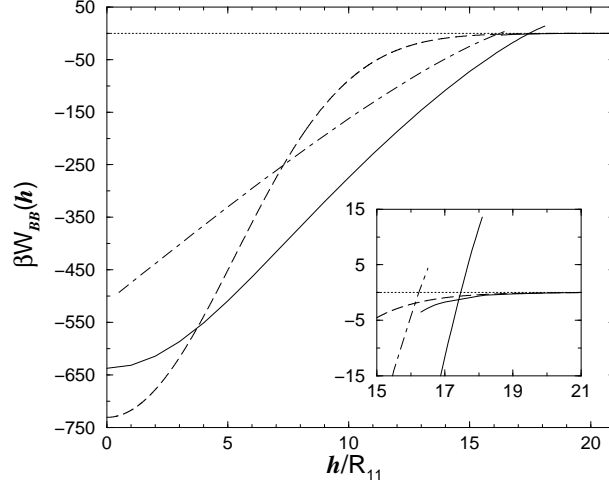
FIG. 6: The SM potential between two big GCM particles in a binary solvent of smaller particles for the same state point as in Figs. 4 and 5, i.e. with total bulk density $\rho^0 R_{11}^3 = 8.5$ and concentration $x = 0.948$. h is the separation between the centres of the two big particles. The dashed line is the result for $W_{BB}(h)$ obtained using the insertion method, the dot-dashed line is the 'sharp-kink' result (see text, Sec. IV) and the solid lines denote the results from the 'brute-force' calculation. In the brute-force calculation, one finds that there are two branches for $W_{BB}(h)$ (see inset for more detail), each with a metastable portion. The branch with the smaller value of $W_{BB}(h)$ is stable. This corresponds to the configuration with no bridge for $h > h_t$, and to the bridged configuration for $h < h_t$. At $h_t/R_{11} = 17.4$, where the two branches cross, there is a discontinuity in the gradient of $W_{BB}(h)$, i.e. there is a jump in the SM force at this separation.

the surface area $A(l, h)$ which appears in the second term.

Using equations (16), (15) and (3) we can obtain an expression for the SM potential:

$$W_{BB}(h) \simeq [A(l, h) - 8\pi l^2]\gamma(\infty). \tag{17}$$

We now present a simple model for $A(l, h)$, (see also Ref. 32) which we expect to be reliable for values of h near to where the bridging transition occurs.

When $h \gg 2l$, i.e. no fluid bridge is present, then $A(l, h) = 8\pi l^2$, and Eq. (17) gives $W_{BB}(h) = 0$. When there is a bridge we approximate the end sections of $A(l, h)$ by the surfaces of two sections of spheres with radius l, and the bridge surface by the surface generated by rotating the arc of a circle, of radius s, about the axis passing through the centres of the end sphere sections (the z-axis). We denote the width along the z-axis of the
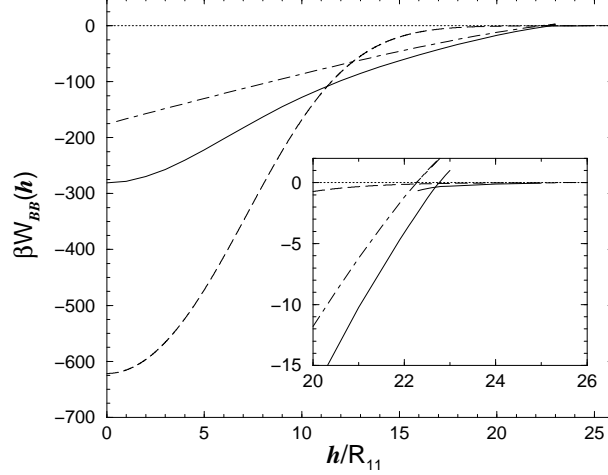
14

FIG. 7: The SM potential between two big GCM particles in a binary solvent of smaller particles near to phase separation, with total bulk density $\rho^0 R_{11}^3 = 6.9$ and concentration $x = 0.88$. h is the separation between the two big particles. The dashed line is the result for the SM potential from the insertion method, the solid lines are the results from the 'brute-force' calculation and the dot-dashed line is the 'sharp-kink' result. In the inset we display a magnification of $W_{BB}(h)$ for large h, showing the two branches crossing at $h_t/R_{11} = 22.7$ and giving rise to a jump in the SM force.

bridge section by $2w$ and the diameter of the bridge section at the mid point between the centres of the end sphere sections by $2d$. The surface area of the two end spherical sections is $4\pi l(l + h/2 - w)$ and the surface area of the bridge section is $4\pi s(s + d)\arcsin(w/s) - 4\pi sw$. Requiring continuity of the surfaces where the end and bridge sections meet and also requiring continuity in the gradients at the point where these sections join, we eliminate s and d to obtain the following expression for the total surface area:

$$A(l, h) = \frac{2\pi\, w\, l\, h}{(h/2 - w)^2}\sqrt{l^2 - (h/2 - w)^2}\,\arcsin\left(\frac{h/2 - w}{l}\right)$$
$$- \frac{4\pi\, w^2\, l}{h/2 - w} + 4\pi\, l\,(l + h/2 - w)\,. \tag{18}$$

We choose the value $w = w_0$ which minimises A, i.e. $\partial A/\partial w|_{w=w_0} = 0$ and use this prescription for calculating $A(l, h)$ with Eq. (17) to calculate the SM potential between two big GCM particles at state points near to coexistence. For the case when the small particle solvent has a total density $\rho^0 R_{11}^3 = 8.5$ and concentration $x = 0.948$, corresponding to the full DFT calculation of the SM potential in Fig. 6, we find that $\beta R_{11}^2 \gamma(\infty) = 0.830$, and

15

that the film thickness $l/R_{11} \simeq 7$ (see Fig. 6 in Ref. 9). Using these values in Eqs. (18) and (17), we calculate the SM potential for this state point. The result is the dot-dashed line displayed in Fig. 6 which is in good qualitative agreement with our results from the full 'brute-force' calculation of the SM potential, particularly for values of h near to where the bridging transition occurs. We also used this simple approximation for the case when the small particle solvent has a total density $\rho^0 R_{11}^3 = 6.9$ and concentration $x = 0.88$, corresponding to the full DFT calculation of the SM potential in Fig. 7. For this state point $\beta R_{11}^2 \gamma(\infty) = 0.152$, and $l/R_{11} = 9.6$ (see Figs. 4 and 9 in Ref. 9) and the SM potential is shown as the dot-dashed line in Fig. 7. Again, the results are in qualitative agreement with those of the full calculation. In particular, this simple approach provides a surprisingly accurate means of estimating the value of h at which the bridging transition will occur. If we assume that bridging will only occur when $W_{BB}(h) < 0$ the resulting values of h_t underestimate the results of the full calculation by only a few percent in both cases. Even for small values of h the results of the sharp-kink approximation for $W_{BB}(h)$ are of the correct magnitude. However, this approximation fails to reproduce the correct shape of $W_{BB}(h)$ for small h.

V.   THICK ADSORBED FILMS ON COMPOSITE PARTICLES

In the previous sections we considered only state points near the binodal where we know that a single big GCM particle is 'wet' by a thick adsorbed film of the coexisting phase rich in species 1, i.e. state points inside or below the single particle thin-thick adsorbed film transition line. However, there can also be pronounced effects on the SM potential due to the presence of thick adsorbed films for state points *outside* the single particle thin-thick adsorbed film transition line (see Fig. 1), where a single big particle immersed in the solvent does not develop a thick adsorbed film. When two big particles are sufficiently close together the resulting composite object can be sufficiently large that a thick film is adsorbed. This effect is somewhat analogous to the case for big hard-core solute particles, where for certain state points for which no thick adsorbed films are present, capillary condensation of the coexisting phase can occur in the space between the two big particles, provided these come sufficiently close together.[4,22] We cannot strictly describe the phenomenon we observe as capillary condensation because the big particles that we consider in the present work have

16

soft cores. Nevertheless, the present phenomenon has a similar effect on the SM potential, i.e. there is a jump in the SM force on reducing the separation h. As mentioned above, this phenomenon occurs outside (but close to) the single particle thin-thick adsorbed film transition line. However, its occurrence is restricted to a particular region of the phase diagram. If one considers two big particles with full overlap ($h = 0$) one can calculate the thin-thick adsorbed film transition line for this composite object. This line is higher in total density than the corresponding single particle transition line (see Fig. 1) and serves as an upper bound for the regime where 'capillary condensation' occurs; the latter is restricted to the region betwen the two transition lines.

The solvent density profiles around two big particles with h sufficiently small that this 'condensation' has occurred are very similar in form to the profiles in Fig. 4, i.e. the 'condensation' does not just occur in the space between the two big particles, as would be the case with a pair of hard-core big particles. Rather, due to the soft core nature of the GCM, the adsorbed film spreads around the whole region in which the two big particles are situated.

In Fig. 8 we display the SM potential between two big GCM particles in a binary solvent of smaller particles with total bulk density $\rho^0 R_{11}^3 = 11$ and concentration $x = 0.983$. This state point is located at bulk coexistence above the single particle thin-thick adsorbed film transition line but inside the transition line for the composite particle – see Fig. 1. For large values of h the SM potential calculated via the 'brute-force' approach is in good agreement with the results from the insertion method. At this state point the insertion method does not include any effects of thick adsorbed films since the inputs into this theory are the density profiles around a single big particle; for this state point a single big particle has no thick adsorbed film. However, as h is decreased the results of the full DFT calculation show that there is a discontinuity in the gradient of $W_{BB}(h)$ due to the formation of a thick adsorbed film around the two particles. The change in the SM potential is very pronounced; the potential becomes much more strongly attractive – see Fig. 8. The insertion method (dashed line) accounts extremely well for the large h behaviour of the SM potential. It also describes accurately the metastable portion of $W_{BB}(h)$ for h below the transition value. However, it fails completely to describe the stable, strongly attractive portion arising from the formation of the thick adsorbed film around the two particles; it underestimates the strength of the attraction by a factor of about 10. This is not too surprising given that this method inputs only the density profiles around a single big particle and that these exhibit
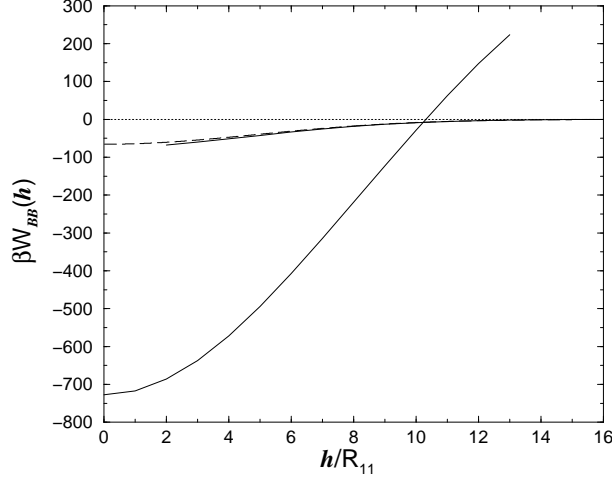
FIG. 8: The SM potential between two big GCM particles in a binary solvent of smaller particles with total bulk density $\rho^0 R_{11}^3 = 11$ and concentration $x = 0.983$ (this state point is at bulk coexistence, outside the single particle thin-thick adsorbed film transition line, but inside the thin-thick adsorbed film transition line for a composite pair of completely overlapping big particles – see Fig. 1). h is the separation between the centres of the two big GCM particles. The dashed line is the result for $W_{BB}(h)$ obtained using the insertion method and the solid lines denote the results from the 'brute-force' method. For this state point a single big particle does not develop thick adsorbed film, but when two big particles are sufficiently close together the resulting composite object can develop a thick adsorbed film. The two branches of $W_{BB}(h)$ correspond to configurations without adsorbed films (stable at large h) and with films (stable at small h). These cross at $h/R_{11} = 10.2$, resulting in a discontinuity in the gradient of $W_{BB}(h)$ and a jump in the SM force.

no thick adsorbed films for this state point.

VI.   BRIDGING AND THE BRIDGE FUNCTION

We recall that the SM potential $W_{BB}(r)$ is related via Eqs. (4) and (5) to the pair correlation function between solute particles, $g_{BB}(r)$, in a bulk ternary mixture which consists of a single, big solute species B and two solvent species, considered in the dilute limit of solute, $\rho_B \to 0$. Since integral equations are a standard tool to determine bulk pair correlation functions in the theory of classical liquids,[26] it is natural to analyse the SM potential within this framework. However, we recall from the outset that whilst integral equation theories

have achieved remarkable precision in the description of one–component bulk fluids, integral equation closure approximations are generally less reliable in multi–component mixtures, especially for situations where the size of one component becomes much larger than the others leading to the possibility of thick film adsorption or wetting phenomena or, in the case of hard-sphere mixtures, to depletion phenomena.

Before we analyse $g_{BB}(r)$ in the ternary mixture, it is instructive to point out some features of the two–component solvent mixture which provide a relationship between the hypernetted chain (HNC) integral equations and the RPA density functional used in the present work. Diagrammatic analysis yields the following standard relationships between the pair correlation functions in a homogeneous (bulk) mixture:[26]

$$h_{ij}(r) - c_{ij}^{(2)}(r) = \sum_{k=1,2} \rho_k^0 \int d\mathbf{r}' h_{ik}(|\mathbf{r} - \mathbf{r}'|) c_{kj}^{(2)}(r'), \tag{19}$$

$$\ln g_{ij}(r) + \beta v_{ij}(r) = h_{ij}(r) - c_{ij}^{(2)}(r) + b_{ij}(r), \tag{20}$$

where $h_{ij}(r) = g_{ij}(r) - 1$. The first equation is the OZ equation for binary mixtures, and the second provides the formally exact closure to the OZ equation in terms of the (generally unknown) bridge function $b_{ij}(r)$. The bulk densities of the two solvent species are denoted by ρ_k^0 ($k = 1, 2$). It is a special feature of the binary GCM (or related soft–core models) that its pair correlation functions are very well described within the HNC approximation[1,12,13,14,15,16,17,18,29,33] which amounts to setting $b_{ij}(r) = 0$. We denote the corresponding solution for the pair direct correlation function by $c_{ij}^{(2),HNC}(r)$. The relation to density functional theory follows by noting that the HNC equations, Eq. (20) with $b_{ij}(r) = 0$, are identical to the test particle equations obtained from a DFT with the excess free energy functional[34]

$$\mathcal{F}_{ex}^{HNC}[\{\rho_i\}] = A_{ex}(\{\rho_i^0\}) + \sum_{i=1,2} \int d\mathbf{r} \mu_i^{HNC} \Delta\rho_i(\mathbf{r}) -$$
$$\frac{1}{2\beta} \int d\mathbf{r} \int d\mathbf{r}' \sum_{ij=1,2} c_{ij}^{(2),HNC}(|\mathbf{r} - \mathbf{r}'|) \Delta\rho_i(\mathbf{r}) \Delta\rho_j(\mathbf{r}'), \tag{21}$$

corresponding to a Taylor expansion to quadratic order in $\Delta\rho_i(\mathbf{r})$ about the bulk densities. The test particle equations follow by choosing as external potentials the interparticle potential $v_{ji}(r)$, minimising the HNC grand potential functional with respect to $\rho_j(r)$ and identifying $g_{ji}(r) \equiv \rho_j(r)/\rho_j^0$. In Eq. (21), $\Delta\rho_i(\mathbf{r}) = \rho_i(\mathbf{r}) - \rho_i^0$ and $A_{ex}(\{\rho_i^0\})$ denotes the

excess Helmholtz free energy of the bulk solvent. The HNC chemical potential is given by

$$\beta\mu_i^{HNC} = \sum_{j=1,2} \rho_j^0 \int d\mathbf{r} \left(\frac{1}{2} h_{ji}(r)[h_{ji}(r) - c_{ji}^{(2),HNC}(r)] - c_{ji}^{(2),HNC}(r) \right) . \tag{22}$$

Previous results for the GCM showed that the pair correlation functions obtained from the HNC were similar to those obtained from the RPA[1,12,13,33] and that the fluid-fluid binodals from the RPA and the HNC approximation were close to each other.[33] If one neglects the weak density dependence of $c_{ji}^{(2),HNC}(r)$ and sets $c_{ji}^{(2),HNC}(r) \simeq c_{ji}^{(2),RPA}(r) = -\beta v_{ji}(r)$ then one can show for the binary mixture, $i = 1, 2$:

$$\mathcal{F}_{ex}^{HNC}[\{\rho_i\}] \simeq \mathcal{F}_{ex}^{RPA}[\{\rho_i\}] \tag{23}$$

where $\mathcal{F}_{ex}^{RPA}$ is the RPA functional defined in Eq. (11).

We have seen in earlier sections that for a fixed big Gaussian particle exerting an external potential on the solvent close to coexistence, the RPA functional accounts for the formation of a thick adsorbed film. It also accounts for complete wetting at a planar wall.[17] Owing to the weak density dependence of $c_{ij}^{(2),HNC}(r)$ we also expect the HNC functional to describe thick film formation and complete wetting. (This is in sharp contrast to simple fluids of the Lennard–Jones type where the harshly repulsive core in the interatomic potential induces a strong density dependence of the direct correlation function $c^{(2)}(r)$ and the HNC functional (21) fails to account for complete wetting[34,35]).

Explicit minimisation of the HNC functional for a binary mixture in the presence of an external potential due to a single solute particle yields the HNC solute–solvent integral equations. These can also be derived from the test particle equations of the HNC functional for the *ternary* mixture of binary solvent plus solute *in the dilute limit* of the solute, $\rho_B \to 0$. This functional is linear in $\rho_B(\mathbf{r})$ and is, at most, quadratic in the other density profiles. It is given by

$$\mathcal{F}_{ex,tern}^{HNC} = \mathcal{F}_{ex}^{HNC} + \mu_B^{HNC} \int d\mathbf{r}\, \rho_B(\mathbf{r})$$
$$- \frac{1}{2\beta} \int d\mathbf{r} \int d\mathbf{r}' \sum_{i=1,2} c_{iB}^{(2),HNC}(|\mathbf{r} - \mathbf{r}'|) \Delta\rho_i(\mathbf{r})\, \rho_B(\mathbf{r}') . \tag{24}$$

Here, $\mu_B(\{\rho_i^0\})$ is the HNC insertion free energy (chemical potential) for inserting a single solute particle into the bulk solvent with densities ρ_i^0 ($i = 1, 2$). Analogously to Eq. (22),

20

μ_B^{HNC} is given by

$$\beta\mu_B^{HNC} = \sum_{i=1,2} \rho_i^0 \int d\mathbf{r} \left(\frac{1}{2} h_{iB}(r)[h_{iB}(r) - c_{iB}^{(2),HNC}(r)] - c_{iB}^{(2),HNC}(r) \right) , \qquad (25)$$

where the solute–solvent pair correlation function $h_{iB}(r)$ and the direct correlation function $c_{iB}^{(2),HNC}(r)$ are determined by solving the solvent–solvent and solute–solvent HNC equations. In the dilute limit of solute, the solute–solvent direct correlation function satisfies the OZ equation

$$c_{iB}^{(2)}(r) = h_{iB}(r) - \sum_{j=1,2} \rho_j^0 \int d\mathbf{r}' h_{Bj}(|\mathbf{r} - \mathbf{r}'|)c_{ji}^{(2)}(r'), \qquad (26)$$

for $i = 1, 2$. In this treatment thick adsorbed films can develop around a big solute particle and this is manifest in the density profiles of the two solvent species and thus in $h_{Bj}(r)$. It follows from Eq. (26) that information about thick films is fed into $c_{iB}^{(2)}(r)$. We can deduce that whenever thick film formation occurs, $c_{iB}^{(2),HNC}(r)$ can be very different from the RPA result $-\beta v_{iB}(r)$.

We turn attention now to the solute–solute correlation functions. These are generated by employing $\mathcal{F}_{ex,tern}^{HNC}$, fixing $v_{BB}(r)$ as the external potential and minimising the grand potential functional with respect to $\rho_B(r)$. One finds

$$\ln g_{BB}(r) + \beta v_{BB}(r) = \sum_{i=1,2} \rho_i^0 \int d\mathbf{r}' h_{Bi}(|\mathbf{r} - \mathbf{r}'|)c_{iB}^{(2),HNC}(r') . \qquad (27)$$

If one now employs the mixture OZ equations in the limit $\rho_B \to 0$ one obtains

$$\ln g_{BB}(r) + \beta v_{BB}(r) = h_{BB}(r) - c_{BB}^{(2)}(r) . \qquad (28)$$

Note that the right hand side of Eq. (27) depends on the solute–solvent correlation functions $h_{Bi}(r)$ and and $c_{iB}^{(2),HNC}(r)$. The former quantity is, essentially, the density profile of species i around a single big particle determined by minimising the HNC functional and the latter is given by the OZ equation (26). One might expect both quantities to be given accurately by the HNC treatment. The $g_{BB}(r)$ resulting from Eq. (27) yields, via Eqs. (4) and (5), an SM potential which we refer to as $W_{BB}^{HNC}(r)$ since this is consistent with the fact that $g_{BB}(r)$ satisfies Eq. (28), the HNC equation for big-big correlations; the latter sets the bridge function $b_{BB}(r) = 0$.

As the HNC inputs only the pair direct correlation functions $c_{ij}^{(2),HNC}(r)$ of the *small* solvent species, which should be well described by their RPA counterparts, we adopt the

following procedure: determine the density profiles of the two small species around a single big particle by minimising the RPA grand potential functional, Eqs. (6) and (11), and use these as input for $h_{Bi}(r)$, along with $c_{ij}^{(2),RPA}(r)$ for the solvent–solvent direct correlation functions, in Eq. (26). The resulting $c_{iB}^{(2)}(r)$ are then used in Eq. (27) to calculate $g_{BB}(r)$ and, hence, the SM potential – which should be very close to $W_{BB}^{HNC}(r)$. We find that $W_{BB}^{HNC}(r)$, for large r, is almost identical to the branch of $W_{BB}(r)$ obtained using the 'brute-force' DFT method presented in Secs. II and III, for which there is *no fluid bridge.* In other words, when there is no fluid bridge, i.e. for $r \equiv h > h_t$, where $h_t = h_t(\rho_1^0, \rho_2^0)$ is the separation at which the bridging transition occurs, $W_{BB}^{HNC}(r) \simeq W_{BB}(r)$ and we can infer that the HNC approximation $b_{BB}(r) \simeq 0$ is valid. However, for $h < h_t$ we find $W_{BB}^{HNC}(r)$ is very different from $W_{BB}(r)$, indicating that the bridge function $b_{BB}(r)$, omitted from this analysis, must be substantial for $h < h_t$. Thus we have demonstrated that $b_{BB}(r)$ must play a significant role in determining the fluid structure when there is bridging.

We conclude that the ternary HNC functional, Eq. (24), describes correctly the bulk solvent–solvent correlations and captures thick film formation in the solute–solvent correlations with a vanishing solute–solvent bridge function, $b_{iB}(r) = 0$. For the solute–solute correlations when bridging is not present the HNC assumption $b_{BB}(r) = 0$ remains accurate but this approximation fails completely when bridging is present. This means that a more sophisticated theory should include in the ternary functional terms proportional to $\rho_B(\mathbf{r}) \, \Delta\rho_i(\mathbf{r}') \, \Delta\rho_j(\mathbf{r}'')$ and higher orders. These will become important near the onset of the transition.

VII. DISCUSSION AND CONCLUSIONS

Using 'brute-force' DFT we have calculated the SM potential $W_{BB}(h)$ between a pair of big GCM particles in a binary solvent of smaller GCM particles. In particular, we have focused on the regime where the big particles are immersed in the binary solvent near to bulk phase separation, where thick films of the coexisting solvent phase adsorbed around the big particles influence strongly the SM potential. It is in this regime that we find bridging transitions. We show that the insertion method for calculating the SM potential used in Refs. 8,9, and which is based on the ternary version of the RPA functional (11), is unable to incorporate the effects of bridging. This method does provide an accurate approximation

for $W_{BB}(h)$ for solvent state points away from the binodal. The bridging that we find is of two types: i) that due to the joining of thick adsorbed films around the individual big particles, described in Sec. III, and ii) that due to local condensation around a pair of particles, described in Sec. V. Both result in a change in slope of $W_{BB}(h)$ at a separation $h = h_t$ and therefore a jump in the SM force at $h = h_t$.

Within our mean-field theory, bridging manifests itself as a sharp (first-order) transition. However, this cannot be the case in reality since the bridging transition involves a finite number of particles and therefore fluctuation effects will round the transition (see discussion in Ref. 4). We can make a crude estimate of the extent of rounding effects by arguing that fluctuations should only be relevant when $|W_{BB}^{\mathrm{br.}}(h) - W_{BB}^{\mathrm{no\,br.}}(h)| \lesssim k_B T$, where $W_{BB}^{\mathrm{br.}}(h)$ denotes the branch of $W_{BB}(h)$ where there is a fluid bridge and $W_{BB}^{\mathrm{no\,br.}}(h)$ the branch without a fluid bridge. From this inequality we can obtain the width, δh_t, over which the transition at h_t will be smeared. We find that $\delta h_t / h_t \sim 10^{-2}$ for the state points corresponding to the SM potentials displayed in Figs. 6 and 7. This measure of the rounding becomes smaller for solvent state points further removed from the bulk critical point. For bigger solute particles we also expect the extent of the rounding to become smaller. At first sight our estimate of the rounding may seem surprisingly small, bearing in mind that the size ratio between the big solute and small solvent particles is only about 7:1. However, due to the soft-core nature of the GCM fluid, the solvent density is high and the number of particles involved in the bridging transition can be large. This demonstrates one of the important differences between the soft-core GCM and more typical hard-core fluid systems: For hard-core particles one would not find thick adsorbed films of the solvent were the size ratio between the solute and solvent only 7:1. Typically the solute must be of order 50 or more times larger than the solvent particles for wetting phenomena to become significant – see also the discussion in Ref. 9.

Our analysis in Sec. VI demonstrates that in order to incorporate bridging into a full (ternary) mixture theory, one must implement an accurate theory for the fluid bridge functions; in particular for the solute-solvent and solute-solute bridge functions $b_{Bi}(r)$ and $b_{BB}(r)$. $b_{BB}(r)$, the solute-solute bridge function, remains little understood but must play a crucial role when there are thick adsorbed films surrounding the big particles. That the bridge functions are required highlights the essential many-body nature of the effective interaction between the big solute particles. Hence, it is not surprising that the insertion method

combined with the ternary version of the RPA functional (11) is unable to incorporate the effects of bridging on the SM potential. We re-iterate that the insertion method is formally exact; it is its use with an approximate functional which leads to neglect of the key features of bridging. In order to obtain insight as to what is required in a theory for the full mixture Helmholtz free energy functional which incorporates the effect of bridging, we consider the exact inhomogeneous Kirkwood-Hill formula[9,36] (recall Eq. (9)):

$$c_B^{(1)}(\mathbf{r}) = -\sum_{\nu=1}^{2} \int_0^1 d\lambda \int d\mathbf{r}' \rho_\nu(\mathbf{r}') g_{B\nu}(\mathbf{r}, \mathbf{r}'; \lambda) \beta v_{B\nu}(|\mathbf{r} - \mathbf{r}'|), \qquad (29)$$

for the one-body direct correlation function of the big solute particles in the limit $\rho_B \to 0$. $v_{B\nu}(r)$ are the big-small pair potentials and the parameter λ, with $0 \le \lambda \le 1$, is used to 'turn on' the effect of the inserted big particle via the potential $\lambda v_{B\nu}(r)$. One calculates the solvent response through the inhomogeneous big-small pair distribution function $g_{B\nu}(\mathbf{r}, \mathbf{r}'; \lambda)$, as λ is increased from 0 to 1. Combining Eq. (29) with Eq. (13) one obtains an exact expression for $W_{BB}(r)$, given by Eq. (70) of Ref. 9. Consider the case when the solvent is near coexistence at a state point below the single big particle thin-thick adsorbed film transition line. If one calculates $W_{BB}(h)$ via Eq. (29), then $g_{B\nu}(\mathbf{r}, \mathbf{r}'; \lambda = 0)$ will correspond to the distribution arising from a fixed single big particle located at $\mathbf{r} = -\mathbf{h}/2$ exerting an external potential on the solvent. This big particle will be surrounded by a thick adsorbed film. Then, 'turning on' the effect of the second big particle (by increasing λ from zero) located at $\mathbf{r} = +\mathbf{h}/2$ one could perhaps envisage the situation where there might be two 'jumps' in $g_{B\nu}(\mathbf{r}, \mathbf{r}'; \lambda)$ for a particular value of $h = |\mathbf{h}|$. The first would be at $\lambda = \lambda_1$, when the potential $\lambda_1 v_{B\nu}(r)$ becomes sufficiently strong to induce condensation of the coexisting solvent phase around this second big particle. This 'jump' in $g_{B\nu}(\mathbf{r}, \mathbf{r}'; \lambda)$ could then be followed by a second jump at $\lambda = \lambda_2$ $(\lambda_1 < \lambda_2 < 1)$, when a fluid bridge forms between the two big particles. That such complex phenomena must be described by $c_B^{(1)}(\mathbf{r})$, which is obtained by taking one functional derivative of the excess Helmholtz free energy functional Eq. (9), attests to the degree of sophistication required in the ternary mixture functional $\mathcal{F}_{ex}[\{\rho_i\}]$ if this is to incorporate bridging. By employing the RPA functional in the insertion approach one incorporates the effect of the thick film surrounding the first big particle via $\rho_\nu(\mathbf{r})$ in Eq. (29), but neglects the effect of the thick film around the second big particle by setting $g_{B\nu}(\mathbf{r}, \mathbf{r}'; \lambda) = 1$ for all λ.[9] One is thereby unable to incorporate the effect of bridging on the SM potential. This point is highlighted further by the case described in Sec. V, where a single big particle has no

thick adsorbed film and the bridging arises from condensation around a *pair* of big particles. In this situation all the information about bridging/wetting must be generated in $c_B^{(1)}(\mathbf{r})$ from a source other than the solvent density profiles around a single big particle, i.e. from subtle correlations in the inhomogeneous solvent. Incorporating such correlations is a tall order for a theory!

The simple capillarity (or sharp-kink) approximation used in Sec. IV to provide an approximate theory for when bridging occurs between two thick adsorbed films seems to be quite good. The simple form, Eq. (17), taken with Eq. (18), is surprisingly reliable in determining an approximation for h_t, the separation between the big particles at which bridging occurs, as well as providing a reasonable approximation for the slope of $W_{BB}(h)$ near the onset of the bridged configuration, i.e. it provides quite a good approximation for the SM force at $h \sim h_t$. The capillarity approximation is not reliable for small h. Here the shape of the SM potential determined from the capillarity approximation is completely wrong, and therefore the SM force obtained from this approximation will be completely unreliable – see Figs. 6 and 7. The 'brute-force' calculation shows that as $h \to 0$, the SM force $\to 0$, whereas the capillarity approximation shows the SM force tending to a non-zero constant value as $h \to 0$. We believe the origin of this failure lies in our simple approximation (18) for the area of the fluid-fluid interface.

One issue we have not raised so far is what does one take for $v_{BB}(r)$, the bare big-big pair potential? This does not enter our calculation of the SM potential, since it is only $v_{B\nu}(r)$, the big-small pair potentials, that are involved; the big particles are treated as external potentials. Therefore, in principle, $v_{BB}(r)$ could take any form, although choosing a bare potential with a hard core would be inconsistent with the soft-core nature of $v_{B\nu}(r)$. A Gaussian potential of the form given in Eq. (1) would seem a natural choice for $v_{BB}(r)$. When one considers the GCM to be a simple model for polymers in solution, then the following empirical rules for the pair potential parameters apply between unlike species:[9,13,16,20] $R_{i \neq j}^2 = (R_{ii}^2 + R_{jj}^2)/2$ and $\epsilon_{i \neq j} < \epsilon_{ii} \simeq \epsilon_{jj}$. Therefore, the choices $R_{BB}/R_{11} = 7$ and $\epsilon_{BB} = 2k_B T$ would be consistent with the parameters we have used for the big-small pair potentials.[9] If we employ a bare Gaussian potential with these parameters the big-big repulsion is negligible when compared to the attractive $W_{BB}(r)$, particularly when there are thick adsorbed wetting films present around the big particles. Thus, the resulting effective pair potential, $v_{BB}^{eff}(r)$, given by Eq. (4) can be very strongly attractive.

If one were seeking to investigate experimentally the effects of thick adsorbed films and bridging between colloidal particles, one approach is to perform light scattering experiments in order to measure the second virial coefficient, B_2.[37] As pointed out in Ref. 9, B_2, which measures the integral of $-r^2(\exp[-\beta v_{BB}^{eff}(r)] - 1)$ should be very large and negative when adsorbed films are present. A rapid change to large negative values of B_2 upon changing the solvent state point should indicate the development of thick adsorbed films around the colloids, thereby influencing the SM potential.[9] Whether B_2 does show a rapid variation with composition in the neighbourhood of the thin-thick transition lines remains to be ascertained.

Finally we note that, just as a pair of big particles with $h = 0$ exhibits a thin-thick adsorbed film transition line, at total densities higher than the single particle thin-thick adsorbed transition line (see Fig. 1), there should also be a thin-thick adsorbed film transition line at even higher densities for three big particles whose centres coincide. This will have implications for the three-body interactions between the big particles. Furthermore, there may be other transition lines corresponding to four, five or more big particles completely overlapping.

Acknowledgements

---

[*] Andrew.Archer@bristol.ac.uk

[1] C.N. Likos, Phys. Reports **348**, 267 (2001).

[2] R. Roth, R. Evans and S. Dietrich, *Phys. Rev. E*, **62** 5360 (2000).

[3] See the review by S. Dietrich in *Phase Transitions and Critical Phenomena* **12**, ed C. Domb and J.L. Lebowitz (London: Academic, 1988) p1.

[4] C. Bauer, T. Bieker and S. Dietrich, Phys. Rev. E **62**, 5324 (2000).

[5] J. N. Israelachvili *Intermolecular and Surface Forces* 2nd ed. (Academic: London, 1992).

[6] K. Lum, D. Chandler, and J. D. Weeks, J. Phys. Chem. B **103**, 4570 (1999).

[7] D. Beysens and T. Narayanan, J. Stat. Phys. **95**, 997 (1999), and references therein.

[8] A.J. Archer, R. Evans and R. Roth, Europhys. Lett., **59**, 526 (2002).

[9] A.J. Archer and R. Evans, J. Chem. Phys., **118**, 9726 (2003).

[10] F.H. Stillinger, J. Chem. Phys. **65**, 3968 (1976).

[11] F.H. Stillinger and D.K. Stillinger, Physica A **244**, 358 (1997).

[12] A. Lang, C.N. Likos, M. Watzlawek and H. Löwen, J. Phys.: Condens. Matter **12**, 5087 (2000).

[13] A.A. Louis, P.G. Bolhuis and J-P. Hansen, Phys. Rev. E **62**, 7961 (2000).

[14] A.A. Louis, P.G. Bolhuis, J-P. Hansen and E.J. Meijer, Phys. Rev. Lett. **85**, 2522 (2000).

[15] P.G. Bolhuis, A.A. Louis, J-P. Hansen and E.J. Meijer, J. Chem. Phys. **114**, 4296 (2001).

[16] A.J. Archer and R. Evans, Phys. Rev. E, **64**, 041501 (2001).

[17] A.J. Archer and R. Evans, J. Phys.: Cond. Matter, **14**, 1131 (2002).

[18] R. Finken, A.A. Louis and J-P. Hansen, J. Stat. Phys, **110**, 1015 (2003).

[19] P.J. Flory and W. Krigbaum, J. Chem. Phys. **18**, 1086 (1950).

[20] J. Dautenhahn and C.K. Hall, Macromolecules **27**, 5399 (1994).

[21] R. Evans, in *Fundamentals of Inhomogeneous Fluids*, edited by D. Henderson (Dekker: New York, 1992), ch.3.

[22] H. Stark, J. Fukuda and H. Yokoyama, Phys. Rev. Lett., **92**, 205502 (2004).

[23] D. Andrienko, P. Patrício and O.I. Vinogradova, J. Chem. Phys., **121**, 4414 (2004).

[24] F. Schlesener, A. Hanke and S. Dietrich, J. Stat. Phys., **110**, 981 (2003).

[25] H.H. von Grünberg and R. Klein, J. Chem. Phys., **110**, 5421 (1999).

[26] J.-P. Hansen and I.R. McDonald *Theory of Simple Liquids* 2nd ed (Academic: London, 1986).

[27] S. Amokrane and J.G. Malherbe, J. Phys.: Condens. Matter, **13**, 7199 (2001).

[28] D. Henderson and M. Plischke, J. Chem. Phys., **97**, 7822 (1992).

[29] A.J. Archer, C.N. Likos and R. Evans, J.Phys.: Cond. Matter, **16**, L297 (2004).

[30] In order to locate the single particle thin-thick adsorbed film transition line, one approach is to calculate density profiles at a series of state points along a particular path in the phase diagram. If one uses as a starting approximation in the numerical (iterative) procedure for calculating the density profiles those profiles corresponding to the previous point on the path, then one finds at some state point there is a jump from a thin to a thick adsorbed film. However, this jump does not occur at the equilibrium transition, rather it occurs at the 'spinodal' for this single particle

thin-thick adsorbed film transition. In order to locate correctly the equilibrium transition line, one must calculate the grand potential corresponding to the profiles with a thick and those with a thin adsorbed film. The proper location for the transition is where these two grand potential curves cross. Near the thin-thick adsorbed film critical point there is little hysteresis and therefore very little difference between the location of the line of equilibrium transitions and the spinodal lines. However, for the present system well away from the critical point, there can be very substantial hysteresis. In Ref. 9 a spinodal line was calculated rather than the true transition line, plotted here in Fig. 1. Similar problems of metastability were elucidated in recent DFT studies of layering transitions for a model colloid-polymer mixture adsorbed at a hard wall.[31]

[31] P.P.F. Wessels, M. Schmidt and H. Löwen, J. Phys.: Condens. Matter, **16**, S4169 (2004).

[32] J. Dzubiella and J.-P. Hansen, J. Chem. Phys., **121**, 5514 (2004).

[33] A. Archer, C. N. Likos, and R. Evans, J. Phys.: Condens. Matter, **14**, 12031 (2002).

[34] M. Oettel, cond-mat/0410185.

[35] R. Evans, P. Tarazona and U. Marini Bettolo Marconi, Molec. Phys. **50**, 993 (1983).

[36] J.R. Henderson, Mol. Phys., **50**, 741 (1983).

[37] See, for example, H. de Hek and A. Vrij, J. Colloid Int. Sci. **88**, 258 (1982).